

FLASH: Fast Landmark Aligned Spherical Harmonic Parameterization for Genus-0 Closed Brain Surfaces*

Pui Tung Choi[†], Ka Chun Lam[†], and Lok Ming Lui[†]

Abstract. Surface registration between cortical surfaces is crucial in medical imaging for performing systematic comparisons between brains. Landmark-matching registration that matches anatomical features, called the sulcal landmarks, is often required to obtain a meaningful 1-1 correspondence between brain surfaces. This is commonly done by parameterizing the surface onto a simple parameter domain, such as the unit sphere, in which the sulcal landmarks are consistently aligned. Landmark-matching surface registration can then be obtained from the landmark aligned parameterizations. For genus-0 closed brain surfaces, the optimized spherical harmonic parameterization, which aligns landmarks to consistent locations on the sphere, has been widely used. This approach is limited by the loss of bijectivity under large deformations and the slow computation. In this paper, we propose FLASH, a fast algorithm to compute the optimized spherical harmonic parameterization with consistent landmark alignment. This is achieved by formulating the optimization problem to \mathbb{C} and thereby linearizing the problem. Errors introduced near the pole are corrected using quasi-conformal theories. Also, by adjusting the Beltrami differential of the mapping, a diffeomorphic (1-1, onto) spherical parameterization can be effectively obtained. The proposed algorithm has been tested on 38 human brain surfaces. Experimental results demonstrate that the computation of the landmark aligned spherical harmonic parameterization is significantly accelerated using the proposed algorithm.

Key words. surface registration, brain cortical surfaces, landmark matching, optimized harmonic registration, Beltrami differential

AMS subject classifications. 65D18, 68U05

DOI. 10.1137/130950008

1. Introduction. Surface registration refers to the process of finding a meaningful 1-1 correspondence between different surfaces. Registration is important in applications, such as medical imaging, which require systematic and accurate comparisons between surface data. For example, in human brain mapping, finding accurate registrations between genus-0 closed cortical surfaces is necessary for disease analysis.

Surface registration algorithms can be divided mainly into two categories: (1) landmark-based surface registration and (2) landmark-free surface registration. Landmark-based registration computes 1-1 mapping between surfaces by matching corresponding salient features on both surfaces. The features, usually called landmarks, are either manually labeled by experts or automatically delineated. Landmark-free registration aims at looking for pointwise correspondence between surface data without landmark constraints. Geometric quantities,

*Received by the editors December 20, 2013; accepted for publication (in revised form) October 17, 2014; published electronically January 13, 2015.

<http://www.siam.org/journals/siims/8-1/95000.html>

[†]Department of Mathematics, The Chinese University of Hong Kong, Shatin, Hong Kong (ptchoi@math.cuhk.edu.hk, kclam@math.cuhk.edu.hk, lmloi@math.cuhk.edu.hk). The third author's research was supported by RGC GRF (CUHK Project ID: 404612) and a CUHK FIS grant (Project ID: 1902036).

such as curvatures, are often used to guide the registration. Landmark-based registration requires more interaction from experts to locate salient features, but more accurate registration results can usually be obtained. In medical imaging, since the accuracy of the registration is crucial, landmark-based registration approaches are often used. For brain registration, it is often desirable to look for a smooth and bijective mapping between brain cortical surfaces that matches sulcal landmarks as much as possible. Sulcal landmarks are important anatomical features on the brain cortical surface, and matching the sulci consistently is a good indicator of the accuracy of the registration. It is therefore necessary to develop efficient and effective algorithms to compute the landmark-matching registration between brain surfaces. More specifically, we focus on surface-based parameterizations with topology preserving landmark constraints.

Different algorithms have been proposed to compute landmark-matching registrations between cortical surfaces. One popular approach is by parameterizing the cortical surface onto a simple parameter domain, such as the unit sphere \mathbb{S}^2 , with landmarks consistently aligned. Once the spherical parameterizations of the brain surfaces are obtained, a diffeomorphic registration between the two surfaces can be easily obtained by performing landmark matching on their parameter spaces. For this purpose, optimized spherical harmonic parameterization with consistent alignment of landmarks on the sphere has been widely used. This approach performs well when deformations are small. However, the bijectivity is often lost when larger deformations occur or when a large number of landmark constraints are enforced. Also, since brain cortical surfaces are made closed by computer scientists, they are genus-0 closed surfaces, and hence minimizing the harmonic energy subject to the landmark constraints becomes a highly nonlinear optimization problem. This results in a long computational time. In this paper, we propose an efficient algorithm, called FLASH, to compute the landmark aligned spherical harmonic parameterization. Using the proposed algorithm, the computation is significantly accelerated and the bijectivity is guaranteed.

2. Previous works. Harmonic maps have been widely used for surface registrations and surface parameterizations [8]. The popularity of harmonic maps is attributed to a number of important factors. First, harmonic maps have a clear physical meaning. Harmonic energy serves as a measure of the total stretching of the map. Second, for genus-0 closed surfaces, harmonic maps are equivalent to conformal maps [20]. Third, the computation of harmonic maps can be done by solving a system of semilinear elliptic PDEs. Fourth, harmonic maps continuously depend on the boundary conditions, and hence one can easily control the harmonic maps by adjusting the boundary conditions. Surveys of the literature on harmonic maps can be found in [4, 5].

The study of the discretization of harmonic maps originates from [6, 7]. In [6], Pinkall and Polthier introduced a discretization of the Dirichlet energy for computing piecewise linear minimal surfaces. Eck et al. [7] proposed a discrete harmonic mapping to approximate the continuous harmonic maps using the finite element method. In [10], Lévy et al. proposed a parameterization method by approximating the Cauchy–Riemann equations using the least-squares method. Alliez et al. [11] introduced the intrinsic parameterizations which minimize the distortion of different intrinsic measures of the surface patches.

Surface conformal parameterization has been extensively applied in various fields since it

Table 1*Several previous works on surface parameterization and registration.*

Methods	Landmark constraints	Bijectivity	Complexity
Finite element approximation of conformal mapping [9, 13]	no	no	linear
Spherical conformal mapping [1]	no	no	nonlinear
Landmark constrained surface conformal mapping [2]	yes	no	nonlinear
Shape-based landmark matching [16]	yes	no	nonlinear
Folding-free global conformal mapping [17]	no	yes	nonlinear
Hyperbolic harmonic mapping for constrained brain surface registration [18]	yes	yes	nonlinear

preserves the local geometry well. Recently, many algorithms for computing surface conformal parameterizations have been developed by different research groups. For instance, Angenent and colleagues (see [9, 13]) proposed a finite element approximation of conformal parameterization. They linearized the Laplace–Beltrami operator and solved a sparse linear system to conformally parameterize brain surfaces. Hurdal and Stephenson [12] proposed an algorithm which uses circle packing to produce “flattened” images of cortical surfaces onto the sphere, the Euclidean plane, and the hyperbolic plane. Gu and Yau (see [14, 1]) introduced a nonlinear algorithm for spherical conformal parameterization. They performed the optimization in the tangent space of the sphere using the gradient descent method. The computation is more stable and accurate. In [17], Lai et al. proposed an approach to obtain a folding-free global conformal mapping.

To obtain more accurate 1-1 correspondences between surfaces, landmark-matching surface registrations have been widely studied. Gu et al. [1] proposed using a Möbius transformation that minimizes the landmark mismatch energy to optimize the spherical conformal parameterization. Lui and colleagues (see [2, 30]) introduced a nonlinear algorithm for landmark-matching registration between two genus-0 closed surfaces. They minimized a combined energy which balances the harmonic energy and the landmark mismatch energy to achieve a landmark aligned registration. Wang et al. [15] proposed a surface parameterization method with landmark constraints using Riemann surface structure. The surface is partitioned into patches with each conformally mapped to a parallelogram. Lui et al. [16] introduced a variational approach to obtain shape-based landmark-matching optimized conformal parameterizations of simply connected open brain surfaces. This is done by representing surface maps with vector fields and reconstructing them through solving an integral flow equation. Later, Shi et al. [18] reported a method to achieve a diffeomorphic landmark constrained registration using hyperbolic harmonic mapping. Table 1 lists several previous works and their properties.

It is noteworthy that there is a large variety of applications of surface registration and parameterization in computer graphics and medical imaging. In particular, there are numerous applications of cortical surface parameterization, including statistical shape analysis, morphometry, and signal processing on brain surfaces.

The highly convoluted structure of human cerebral cortices is a major obstacle for physicians in viewing the functional activity on them. To solve this issue, many research groups have proposed different mathematical tools. Thompson and Toga [32] proposed a surface-based technique to perform cortical surface mapping. Later, the use of spherical parameterization of cortical surfaces became widespread in surface-based medical analysis as it enhances the visualization of functional activation taking place on the brain surface [28]. In addition, landmark-based surface registration has been widely applied in brain mapping research. Sulci and gyri, which are fissures and ridges on the surface of a brain, respectively, are frequently used in brain mapping research to perform cortical registration [34, 35, 36]. They are usually regarded as landmarks to make a reliable subdivision of the cortex. Joshi et al. [33] performed surface constrained volumetric brain registration by first parameterizing and aligning the cortical surfaces using sulcal landmarks. Interestingly, sulcal variability and cortical morphometry are closely related. For example, the cortical thickness and volume of the medial frontal lobes are associated with the morphologic characteristics of the paracingulate sulcus [22, 23]. Sulci and gyri are also commonly used in analyzing diseases. For instance, some sulci may have a larger opening and smaller depth in Alzheimer’s patients. Numerous studies have been devoted to understanding Alzheimer’s disease via sulcal variability of brains [25]. In addition, Williams syndrome can also be characterized by abnormal brain structures. Sulcal morphometry has been carried out to study cortical folding abnormalities in the cortex of subjects with Williams syndrome [26, 27]. Sulcal patterns have also been studied using surface-based morphometry methods to predict the locations of Brodmann areas [24]. These medical applications reflect the significance of landmark aligned cortical surface parameterizations.

3. Contributions. The contributions of our work are two-fold. First, we propose a fast and accurate method for spherical conformal parameterization of genus-0 closed brain surfaces. Second, we propose an efficient algorithm for landmark aligned spherical harmonic parameterization of genus-0 closed brain surfaces with bijectivity guaranteed.

For the state-of-the-art approaches for spherical conformal parameterization, the major unsolved issue is the slow computation. We conquer this problem by introducing a fast and accurate method which is 5000 times faster than the conventional method [1]. Angenent and colleagues (see [9, 13]) suggested linearizing the problem by projecting the cortical surface to an open region on the complex plane. A critical drawback of the method is that there is a large conformality distortion near the north pole, which severely affects the accuracy of the parameterization. We improve the method by fixing the conformality distortion using quasi-conformal theories. This is achieved by introducing a north pole–south pole iterative scheme. With the iterative scheme, we linearize the problem on a big triangle on \mathbb{C} and fix the conformality distortion by applying a composition of quasi-conformal mappings on \mathbb{C} . Also, we overcome the problem of nonuniform density due to the stereographic projection by defining the optimal big triangle size. We develop a method to find an optimal size of the big triangle that effectively prevents the points from concentrating at one pole on \mathbb{S}^2 . In summary, by linearizing the problem on a big triangle with the optimal size and by introducing a north pole–south pole iterative scheme, we obtain a fast and accurate spherical conformal parameterization.

For landmark aligned spherical harmonic parameterization, two major limitations of the existing approaches are the slow computation and the loss of bijectivity. To overcome the first limitation, we linearize the model reported by Lui et al. [2] on a big triangle on \mathbb{C} . This significantly speeds up the computation. For the second limitation, it is noteworthy that overlaps usually occur near the sulcal landmark constraints for the existing methods [2, 15], which causes inaccuracies for medical applications. We further introduce an iterative algorithm to efficiently fix the overlaps by adjusting the Beltrami differential. For updating the Beltrami differential, we propose an energy functional with a special weighted term for controlling the movements of the points near ∞ on $\bar{\mathbb{C}}$. This important term avoids large changes in the conformality distortion of the points near the origin. To summarize, we linearize the computation of landmark-matching spherical harmonic parameterization on \mathbb{C} to speed up the computation, and introduce an iterative algorithm with special treatments near ∞ on $\bar{\mathbb{C}}$ to ensure the diffeomorphic property of the parameterization.

4. Our proposed method. In this section, we describe in detail our proposed algorithm for fast landmark aligned spherical harmonic parameterizations of brain surfaces.

One main challenge of the problem is that cortical surfaces are highly convoluted. The complicated geometry of the brain surfaces causes computational difficulties. To simplify the problem, spherical conformal parameterizations can be applied so that all computations can be carried out on \mathbb{S}^2 . Suppose that S_1 and S_2 are two cortical surfaces to be registered. The spherical conformal parameterizations of S_1 and S_2 are first computed, and are denoted by $\phi_1 : S_1 \rightarrow \mathbb{S}^2$ and $\phi_2 : S_2 \rightarrow \mathbb{S}^2$, respectively. Let $\{p_i \in S_1\}_{i=1}^n$ and $\{q_i \in S_2\}_{i=1}^n$ be the corresponding landmark constraints on S_1 and S_2 , respectively. Our problem can be reformulated as finding an optimized harmonic map $\tilde{f} : \mathbb{S}^2 \rightarrow \mathbb{S}^2$ of \mathbb{S}^2 such that $\tilde{f}(\phi_1(p_i)) = \phi_2(q_i)$ for $i = 1, 2, \dots, n$. The optimized harmonic map between S_1 and S_2 can then be obtained by $f := \phi_2^{-1} \circ \tilde{f} \circ \phi_1$. However, this approach is still time-consuming. First, accurately computing the spherical parameterization takes time. Although some relatively fast algorithms have been proposed recently (such as [17]), they still involve the minimization of the harmonic energy on the Riemann surface, which is nonlinear. Second, the optimization problem to obtain the optimized harmonic map between the unit spheres that align landmarks is also nonlinear, which again results in a long computational time. Finally, the optimized harmonic map may not be bijective. Flips or overlaps can often be observed when the displacements of landmarks are not small enough. This causes inaccuracies in the final registration. In this paper, we propose algorithms to

1. speed up the accurate computation of the spherical conformal parameterization;
2. speed up the computation of the landmark aligned spherical harmonic map;
3. enforce the bijectivity of the landmark aligned parameterization.

4.1. Fast spherical parameterization of genus-0 closed surfaces. We first consider a fast algorithm to compute spherical parameterizations $\phi_i : S_i \rightarrow \mathbb{S}^2$ ($i = 1, 2$). A map $f : M \rightarrow N$ between two Riemann surfaces is said to be *conformal* if there exists a positive scalar function u such that $f^*ds_N^2 = u ds_M^2$. It is easy to observe that every conformal map preserves angles. The *harmonic energy functional* for $f : M \rightarrow \mathbb{S}^2$ is defined as

$$(4.1) \quad E(f) = \int_M |\nabla f|^2 dv_M.$$

In the space of mappings, the critical points of $E(f)$ are called *harmonic mappings*. For genus-0 closed surfaces, a conformal map is equivalent to a harmonic map. For more details, please refer to [19, 20]. By the Riemann mapping theorem, every genus-0 closed surface S_i can be conformally mapped onto \mathbb{S}^2 . Also, a conformal map between two genus-0 closed surfaces can be uniquely determined, provided that three-point correspondences are given. Therefore, the conformal parameterization of $\phi_i : S_i \rightarrow \mathbb{S}^2$ can be obtained by solving the following Laplace equation on S_i :

$$(4.2) \quad \Delta_{S_i}^T \phi_i = 0$$

(where $\Delta_{S_i}^T \phi_i$ is the tangential component of $\Delta_{S_i} \phi_i$ on the tangent plane of \mathbb{S}^2), subject to the constraints: (i) $\|\phi_i\| = 1$, and (ii) $\phi_i(p_1^i) = q_1^i$, $\phi_i(p_2^i) = q_2^i$, and $\phi_i(p_3^i) = q_3^i$, and $p_1^i \in S_i$, $p_2^i \in S_i$, $p_3^i \in S_i$, $q_1^i \in \mathbb{S}^2$, $q_2^i \in \mathbb{S}^2$, $q_3^i \in \mathbb{S}^2$. Note that the operator $\Delta_{S_i}^T$ is nonlinear. Thus, solving (4.2) subject to the constraints is time-consuming.

To alleviate this issue, Angenent and colleagues (see [9, 13]) proposed to formulate the spherical parameterization problem to a planar conformal parameterization problem and thereby linearize the problem. By removing a point p_1^i on S_i , $S_i \setminus \{p_1^i\}$ can be conformally mapped onto $\mathbb{S}^2 \setminus \{\phi_i(p_1^i)\}$, which can be further mapped conformally to \mathbb{C} (p_1^i can be considered as being mapped to ∞). In other words, there exists a conformal parameterization $\varphi_i : S_i \setminus \{p_1^i\} \cong \mathbb{C} \rightarrow \mathbb{C}$ such that $\lim_{x \rightarrow p_1^i} \varphi_i(x) = \infty$. φ_i can then be computed by solving the Laplace equation

$$(4.3) \quad \Delta_{S_i} \varphi_i = 0,$$

given three-point correspondences $\varphi_i(a_1^i) = b_1^i$, $\varphi_i(a_2^i) = b_2^i$, and $\varphi_i(a_3^i) = b_3^i$, where $a_1^i, a_2^i, a_3^i, b_1^i, b_2^i, b_3^i \in \mathbb{C}$. Here $\Delta_{S_i}^T = \Delta_{S_i}$ since the target domain is now \mathbb{C} .

The new problem (4.3) is linear since Δ_{S_i} is linear and the nonlinear constraint (i) in the original problem (4.2) is removed. In the discrete case, Δ_{S_i} can be discretized as a symmetric positive definite matrix. Hence, (4.3) can be efficiently solved by the conjugate gradient method. A conformal parameterization $\phi_i : S_i \rightarrow \mathbb{S}^2$ can then be obtained by composing φ_i with the inverse stereographic projection P_N^{-1} . Here, the stereographic projection is defined by $P_N(x, y, z) = (\frac{x}{1-z}, \frac{y}{1-z})$ for any $(x, y, z) \in \mathbb{S}^2 \setminus (0, 0, 1)$.

Despite the fast computation, the method proposed in [9, 13] has a critical drawback in that conformality distortions are often induced near the puncture p_1^i (or a triangular face in the discrete case). The main reason is that the area near the puncture is significantly enlarged when it is mapped to \mathbb{C} through the stereographic projection. In the actual numerical computation, unless the triangulation near the puncture is very dense, numerical errors and thus conformality distortions are usually introduced near p_1^i (see Figure 1). To solve this problem, we propose to improve the conformality distortion of the map near the puncture by composing it with a quasi-conformal map $g_i : \mathbb{S}^2 \rightarrow \mathbb{S}^2$. Quasi-conformal maps are the generalizations of conformal maps, which are orientation preserving homeomorphisms between Riemann surfaces with bounded conformality distortions, in the sense that their first order approximations take small circles to small ellipses of bounded eccentricity [21]. Mathematically, $f : \mathbb{C} \rightarrow \mathbb{C}$ is a *quasi-conformal map* if it satisfies the Beltrami equation

$$(4.4) \quad \frac{\partial f}{\partial \bar{z}} = \mu(z) \frac{\partial f}{\partial z}$$

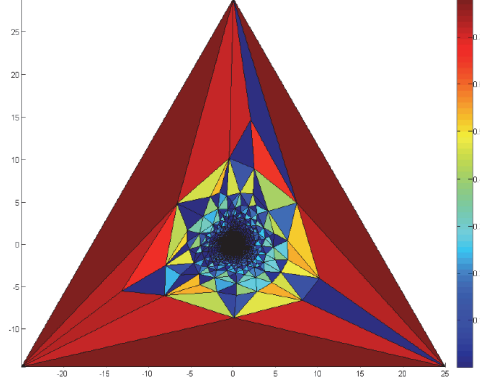


Figure 1. An illustration of how the conformality distortions are introduced near the puncture. Here, the outer region of the big triangle corresponds to the region near the puncture of the mesh. The colormap represents the norm of the Beltrami differential of the map from the big triangle to the original mesh. The red color on the triangular faces in the outer region of the big triangle indicates the large conformality distortions introduced near the puncture.

for some complex-valued functions μ with $\|\mu\|_\infty < 1$. μ is called the *Beltrami coefficient* of f . The Beltrami coefficient measures the conformality distortion of a map. In particular, f is conformal around a small neighborhood of p if and only if $\mu(p) = 0$.

A quasi-conformal map can also be defined between two Riemann surfaces. In this case, a *Beltrami differential* is used. A Beltrami differential $\mu(z) \frac{\bar{dz}}{dz}$ on a Riemann surface S is an assignment to each chart (U_α, ϕ_α) of an L_∞ complex-valued function μ_α , defined on local parameter z_α such that $\mu_\alpha \frac{dz_\alpha}{dz_\alpha} = \mu_\beta \frac{dz_\beta}{dz_\beta}$, on the domain which is also covered by another chart (U_β, ϕ_β) . Here, $\frac{dz_\beta}{dz_\alpha} = \frac{d}{dz_\alpha} \phi_{\alpha\beta}$ and $\phi_{\alpha\beta} = \phi_\beta \circ \phi_\alpha$. An orientation preserving diffeomorphism $f : M \rightarrow N$ is called quasi-conformal associated with $\mu(z) \frac{\bar{dz}}{dz}$ if, for any chart (U_α, ϕ_α) on M and any chart (U_β, ψ_β) on N , the mapping $f_{\alpha\beta} := \psi_\beta \circ f \circ \phi_\alpha^{-1}$ is quasi-conformal associated with $\mu_\alpha \frac{dz_\alpha}{dz_\alpha}$. Readers are referred to [21] for more details about quasi-conformal theories.

Intuitively, composing two maps with the same Beltrami differential cancels out the conformality distortion. In our case, let μ be the Beltrami differential of ϕ_i^{-1} , where $\phi_i : S_i \rightarrow \mathbb{S}^2$ is obtained by solving (4.3). Since significant conformality distortions are introduced near the pole (or $\infty \in \bar{\mathbb{C}}$), $\mu(z)$ is large if z is close to ∞ . In contrast, a negligible conformality distortion is introduced near the south pole. Hence, $\mu(z) \approx 0$ when z is close to 0. We proceed to look for a quasi-conformal map $g : \mathbb{S}^2 \rightarrow \mathbb{S}^2$ with the same Beltrami differential μ . The composition map, $\tilde{\phi}_i := g \circ \phi_i^{-1} : S_i \rightarrow \mathbb{S}^2$, is then conformal. This can be explained by the following theorem.

Theorem 4.1. *Let $f : M_1 \rightarrow M_2$ and $g : M_2 \rightarrow M_3$ be quasi-conformal maps. Suppose the Beltrami differentials of f^{-1} and g are the same. Then the Beltrami differential of $g \circ f$ is equal to 0. Hence, $g \circ f : M_1 \rightarrow M_3$ is conformal.*

Proof. Note that $\mu_{f^{-1}} \circ f = -(f_z/|f_z|)^2 \mu_f$. Since $\mu_{f^{-1}} = \mu_g$, we have

$$(4.5) \quad \mu_f + \frac{\bar{f}_z}{f_z} (\mu_g \circ f) = \mu_f + \frac{\bar{f}_z}{f_z} (\mu_{f^{-1}} \circ f) = \mu_f + \frac{\bar{f}_z}{f_z} \left(-\frac{f_z}{\bar{f}_z} \right) \mu_f = 0.$$

Hence, by the composition formula,

$$(4.6) \quad \mu_{g \circ f} = \frac{\mu_f + \overline{f_z}/f_z(\mu_g \circ f)}{1 + \overline{f_z}/f_z \overline{\mu_f}(\mu_g \circ f)} = 0.$$

Thus, $g \circ f$ is conformal. \blacksquare

Of course, one crucial issue is to efficiently compute g_i . Note that finding a quasi-conformal map on the unit sphere is nonlinear and the computation would be slow. Instead, we desire a fast algorithm to compute the quasi-conformal maps.

Lui et al. [3] proposed a linear algorithm, called the linear Beltrami solver (LBS), to reconstruct a quasi-conformal map g_i from its Beltrami coefficient $\mu = \rho + i\tau$ on rectangular domains in \mathbb{C} . The brief idea is as follows. Let $g_i = u + iv$. From the Beltrami equation (4.4), one can easily check that u and v satisfy the following elliptic PDEs:

$$(4.7) \quad \nabla \cdot \left(A \begin{pmatrix} u_x \\ u_y \end{pmatrix} \right) = 0 \quad \text{and} \quad \nabla \cdot \left(A \begin{pmatrix} v_x \\ v_y \end{pmatrix} \right) = 0,$$

where

$$A = \begin{pmatrix} \alpha_1 & \alpha_2 \\ \alpha_2 & \alpha_3 \end{pmatrix}, \quad \alpha_1 = \frac{(\rho - 1)^2 + \tau^2}{1 - \rho^2 - \tau^2}, \quad \alpha_2 = -\frac{2\tau}{1 - \rho^2 - \tau^2}, \quad \alpha_3 = \frac{1 + 2\rho + \rho^2 + \tau^2}{1 - \rho^2 - \tau^2},$$

and u and v satisfy certain boundary conditions. In the discrete case, solving the above elliptic PDEs (4.7) can be discretized into solving a sparse symmetric positive definite linear system. Readers are referred to [3] for details.

It is noteworthy that the linear algorithm introduced by [3] works only for rectangular domains. The linearity ensures the efficiency of the reconstruction of quasi-conformal maps. Later, Lui and Wen [31] extended the method to hyperbolic domains. Because of the periodic boundary conditions on the hyperbolic domains, the computation is nonlinear. As our focus is on genus-0 closed brain surfaces, which are conformally equivalent to \mathbb{S}^2 , we apply the method to the spherical case, with reasonable computational time. Note that if the elliptic PDEs are solved on the cortical surfaces or the spheres, the problem will be nonlinear. In our work, we use the stereographic projection to turn the problem from solving on the sphere to solving on a big triangle on \mathbb{C} . This linearizes the problem for the spherical case, although distortions are induced near the pole under the stereographic projection. To alleviate this issue, we also use a north pole–south pole iterative scheme to correct the conformality distortion on the spherical parameterizations in linear time.

Now we are ready to propose a north pole–south pole iterative scheme to efficiently obtain an accurate conformal parameterization. Our iterative scheme has two major stages. For the first stage, we apply the method introduced by Angenent and colleagues (see [9, 13]). In particular, in (4.3), we set $[b_1^i, b_2^i, b_3^i]$ to be a big triangle on \mathbb{C} containing the origin that shares the same angle structure as the north pole triangle $[a_1^i, a_2^i, a_3^i]$. The second stage aims to fix the conformality distortion near the north pole. We first project \mathbb{S}^2 conformally onto the complex plane through the south pole stereographic projection P_S , so that $(0, 0, -1)$ is mapped to ∞ , in order to linearize the problem. Our problem is then reduced to finding a quasi-conformal map $\tilde{g}_i : \mathbb{C} \rightarrow \mathbb{C}$ with Beltrami differential $\tilde{\mu}$, where $\tilde{\mu}$ is the Beltrami

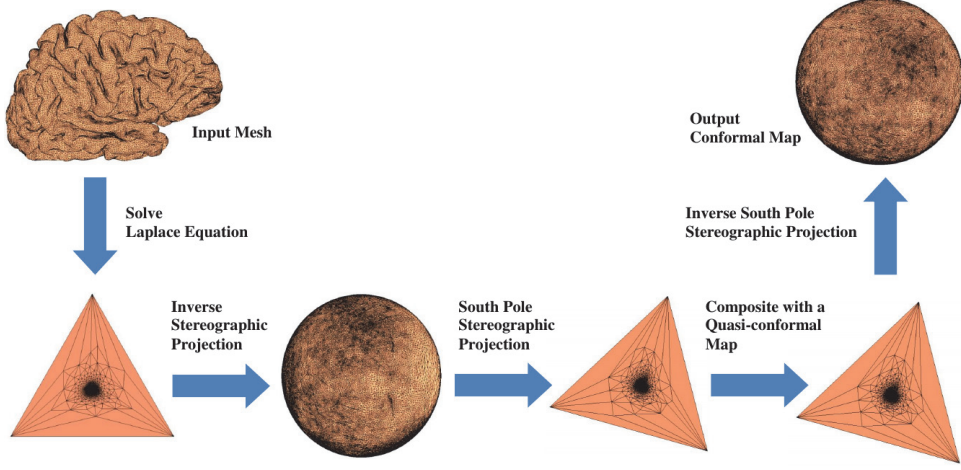


Figure 2. Illustration of our proposed Algorithm 1.

differential of $(P_S \circ \phi_i)^{-1}$. The required quasi-conformal map g_i can then be obtained by $g_i := P_S^{-1} \circ \tilde{g}_i \circ P_S$. However, the south pole stereographic projection will again introduce undesired conformality distortions near the south pole. To solve this problem, we make use of an observation that $\mu \approx 0$ near $(0, 0, -1) \in \mathbb{S}^2$. Therefore, we can fix a small region Ω_S enclosing the south pole, which corresponds to an outer region Ω_C in \mathbb{C} after it is projected onto the two-dimensional plane using P_S . In other words, we look for a quasi-conformal map \tilde{g}_i by solving (4.7) such that

$$(4.8) \quad \begin{aligned} \tilde{g}_i|_{\Omega_C} &= \mathbf{id}|_{\Omega_C}, \\ \mu(\tilde{g}_i)|_{\mathbb{C} \setminus \Omega_C} &= \tilde{\mu}|_{\mathbb{C} \setminus \Omega_C}, \end{aligned}$$

where $\mu(\tilde{g}_i)$ is the Beltrami differential of \tilde{g}_i .

By this treatment, the conformality distortion of $g_i \circ \phi_i$ near the south pole, which is negligible, will remain unchanged. On the other hand, the conformality distortions near the north pole can be much improved, based on Theorem 4.1 (see Figure 5). In addition, all steps in our algorithm, including solving the harmonic equation on \mathbb{C} , the stereographic projections, and the reconstruction of quasi-conformal maps on \mathbb{C} , are linear. Thus, the computations are fast. Figure 2 illustrates the procedure of this algorithm.

In practice, despite the conformality distortions, another serious problem is the density of the vertices on \mathbb{S}^2 . If the big triangle $[b_1^i, b_2^i, b_3^i]$ in (4.3) is too large (or too small), the vertices will concentrate near the north pole (or the south pole) after the inverse stereographic projection. This affects the quality of the spherical parameterization. To solve this problem, we propose to find an optimal big triangle size for a more even distribution. We first observe the following invariance.

Theorem 4.2. *Let T_1 and T_2 be two triangles of \mathbb{C} . The product of the perimeters of T_1 and $P_S(P_N^{-1}(T_2))$ is invariant under arbitrary scaling of T_1 and T_2 .*

Proof. Denote the vertices of T_1, T_2 by $\{a_i\}_{i=1}^3, \{b_i\}_{i=1}^3$, respectively. Note that

$$(4.9) \quad P_S(P_N^{-1}(X + iY)) = \frac{-\frac{2X}{1+X^2+Y^2}}{1 + \frac{-1+X^2+Y^2}{1+X^2+Y^2}} + i \frac{\frac{2Y}{1+X^2+Y^2}}{1 + \frac{-1+X^2+Y^2}{1+X^2+Y^2}} = \frac{-X}{X^2 + Y^2} + i \frac{Y}{X^2 + Y^2}.$$

Hence the perimeter of T_1 is given by $p(T_1) = \sum_{1 \leq i < j \leq 3} |a_i - a_j|$ and $p(P_S(P_N^{-1}(T_2))) = \sum_{1 \leq i < j \leq 3} \left| \frac{-\bar{b}_i}{|b_i|^2} - \frac{-\bar{b}_j}{|b_j|^2} \right|$. Now suppose that T_1 and T_2 are scaled by a factor k . Then

$$(4.10) \quad \begin{aligned} p(kT_1) \times p(P_S(P_N^{-1}(kT_2))) &= \left(\sum_{1 \leq i < j \leq 3} |ka_i - ka_j| \right) \left(\sum_{1 \leq i < j \leq 3} \left| \frac{-\overline{kb}_i}{|kb_i|^2} - \frac{-\overline{kb}_j}{|kb_j|^2} \right| \right) \\ &= \left(k \sum_{1 \leq i < j \leq 3} |a_i - a_j| \right) \left(\frac{1}{k} \sum_{1 \leq i < j \leq 3} \left| \frac{-\bar{b}_i}{|b_i|^2} - \frac{-\bar{b}_j}{|b_j|^2} \right| \right) = p(T_1) \times p(P_S(P_N^{-1}(T_2))). \end{aligned}$$

Hence, the product is an invariance. \blacksquare

Now we apply Theorem 4.2 on the big triangle T and the innermost triangle t on \mathbb{C} , which correspond to the north pole triangle and the south pole triangle on \mathbb{S}^2 . Given an arbitrary big triangle of size s , we define the *optimal big triangle size* by

$$s \times \frac{\sqrt{\text{perimeter}(T) \times \text{perimeter}(P_S(P_N^{-1}(t)))}}{\text{perimeter}(T)}.$$

By the scaling factor, the two triangles T and $P_S(P_N^{-1}(t))$ will have the same perimeter, which indicates that the two polar triangles are of similar size. As a result, the points will not concentrate at one pole.

4.2. Landmark aligned harmonic parameterization. Given two cortical surfaces, we now describe an algorithm to obtain their spherical parameterizations such that their corresponding sulcal landmarks are mapped to consistent locations. Such a parameterization is called a *landmark aligned spherical parameterization*. Once the landmark aligned spherical parameterizations are computed, a landmark-matching registration between the two cortical surfaces can be obtained.

Denote the corresponding landmark curves on S_1 and S_2 by $\{p_i\}_{i=1}^n$ and $\{q_i\}_{i=1}^n$, respectively. To register S_1 and S_2 with landmarks consistently matched, we first apply the aforementioned algorithm to obtain the spherical conformal parameterizations $\phi_1 : S_1 \rightarrow \mathbb{S}^2$ and $\phi_2 : S_2 \rightarrow \mathbb{S}^2$. Denote the two spheres $\phi_1(S_1)$ and $\phi_2(S_2)$ by B_1 and B_2 , respectively. Our goal is to look for an adjusted spherical parameterization of S_1 , $\tilde{\phi}_1 : S_1 \rightarrow \mathbb{S}^2$ such that $\tilde{\phi}_1(p_i) = \phi_2(q_i)$ for $i = 1, 2, \dots, n$. A landmark-matching surface registration between S_1 and S_2 can then be obtained by $f := \phi_2^{-1} \circ \tilde{\phi}_1$.

However, we note that the corresponding landmark curves are mapped to quite different locations on the spheres. Hence, it is undesirable to directly compute the landmark aligned optimized harmonic parameterization, since handling large deformations may be very difficult. To overcome this issue, Gu and Yau (see [1]) proposed to find a suitable Möbius transformation that minimizes a landmark mismatch functional. Let $T = \frac{az+b}{cz+d}$ with $ad - bc = 1$ be a Möbius

transformation of \mathbb{S}^2 . Here \mathbb{S}^2 is identified with $\overline{\mathbb{C}}$ through the stereographic projection. Assume that the landmark curves are represented by discrete landmark points. The landmark mismatch functional [1] is defined by

$$(4.11) \quad E_{MT}(a, b, c, d) = \sum_{i=1}^n |T(\phi_1(p_i)) - \phi_2(q_i)|^2.$$

By adding another constraint for T such that it maps ∞ to ∞ , the energy functional (4.11) can be simplified as

$$(4.12) \quad \tilde{E}_{MT}(a, b) = \sum_{i=1}^n g(\phi_1(p_i)) |a(\phi_1(p_i)) + b - \phi_2(q_i)|^2,$$

where $g(z) = \frac{4}{1+z\bar{z}}$. It remains to look for $a, b \in \mathbb{C}$ such that the energy functional (4.12) is minimized. More details can be found in [1].

As the transformation is restricted to be conformal, the landmarks cannot be exactly aligned in most cases. Nevertheless, we use it as an initial step before further matching and denote the sphere obtained under the optimal Möbius transformation by $\tilde{B}_1 := T(B_1)$. The parameterization can be further adjusted to better align landmarks by solving an optimization problem. More specifically, we can look for a map $\tilde{\phi}_1 : \mathbb{S}^2 \rightarrow \mathbb{S}^2$ that solves the following optimization problem:

$$(4.13) \quad \text{Minimize } E(\tilde{\phi}_1) = \int_{\mathbb{S}^2} |\nabla_{\mathbb{S}^2} \tilde{\phi}_1|_{\mathbb{S}^2}^2$$

subject to the constraint that $\tilde{\phi}_1(\phi_1(p_i)) = \phi_2(q_i)$. Minimizing the energy functional is equivalent to solving

$$(4.14) \quad \Delta_{\mathbb{S}^2}^T \tilde{\phi}_1 = 0$$

subject to the landmark constraints, where $(\Delta_{\mathbb{S}^2})^T \tilde{\phi}_1$ is the tangential component of $\Delta_{S_i} \tilde{\phi}_1$. Lui and colleagues (see [2, 30]) proposed the following combined energy to balance the conformality and the landmark mismatch energy:

$$(4.15) \quad E_{combined}(\tilde{\phi}_1) = \int |\Delta_{\mathbb{S}^2}^T \tilde{\phi}_1|^2 + \lambda \int |\tilde{\phi}_1(\phi_1(p_i)) - \phi_2(q_i)|^2,$$

where λ is a weighting factor. The advantage of using this combined energy is that one can easily adjust the weight between the two energy terms. If $\lambda = 0$, this is exactly the harmonic energy. If λ is large, the landmark mismatch energy will be significantly reduced but more conformality will be lost.

However, in [2, 30], this optimization problem is solved by the gradient descent method, which iteratively finds a vector field in the tangent space of the sphere. Since $\Delta_{\mathbb{S}^2}^T$ is a nonlinear operator on \mathbb{S}^2 , the computation is inefficient. In this work, our approach is to make use of this combined energy but solve the problem in a more efficient way.

Here, we propose a linear algorithm to solve the above optimization problem. The key idea is to formulate the problem on $\overline{\mathbb{C}}$ using the stereographic projection so as to linearize the problem. First, by the stereographic projection, $\tilde{B}_1 \setminus \Omega$ and $B_2 \setminus \Omega$ can be conformally mapped to C_1 and C_2 in \mathbb{C} , respectively, where Ω is a tiny region enclosing $(0, 0, 1) \in \mathbb{S}^2$. Let $\varphi : C_1 \rightarrow \mathbb{C}$ be the landmark constrained harmonic parameterization, and let $\{\tilde{p}_i\}_{i=1}^n$ and $\{\tilde{q}_i\}_{i=1}^n$ be the corresponding landmark curves on C_1 and C_2 , respectively. Given three-point correspondences $\varphi(a_1) = a_1$, $\varphi(a_2) = a_2$, and $\varphi(a_3) = a_3$ on C_1 , φ can be computed by solving the following equation:

$$(4.16) \quad \Delta_{\mathbb{R}^2} \varphi + \lambda \delta_E(\varphi - \tilde{q}_i) = 0,$$

where $\delta_E(w)$ is the smooth approximation of the characteristic function

$$(4.17) \quad \chi_E(w) = \begin{cases} 1 & \text{if } w \text{ is on } \tilde{p}_i, \\ 0 & \text{otherwise.} \end{cases}$$

$\Delta_{\mathbb{R}^2}$ is a linear differential operator. In the discrete case, (4.16) can be discretized into a sparse linear system, which can be efficiently solved by the conjugate gradient method (see section 5.2).

4.3. Preservation of bijectivity via Beltrami differentials. We are concerned about not only the efficiency but also the bijectivity. The bijectivity of the landmark aligned spherical harmonic parameterization is crucial in practical applications. For very large deformations or a large number of landmark constraints, the landmark aligned harmonic parameterization obtained by solving the optimization problem proposed in [2, 30] may not be a diffeomorphism. Here, we look for a method to enforce the bijectivity.

We propose an iterative algorithm to obtain the diffeomorphic property of the resulting map using quasi-conformal theories. Recall that f is a diffeomorphism if and only if $\|\mu_f\|_\infty < 1$, where μ_f is the Beltrami differential of f . By chopping down the norm of the Beltrami differential, if necessary, the diffeomorphic property of the corresponding map can be easily achieved.

Lui and Wen [31] also proposed an iterative algorithm for obtaining a bijective registration using the Beltrami differentials of the surface map. The key step of the method is to smoothen the Beltrami differential by minimizing an energy functional which consists of a gradient term and a penalty term:

$$(4.18) \quad \int |\nabla \mu|^2 + \frac{\lambda}{2} \int |\mu - \mu_n|^2.$$

However, this does not suit our case as our problem is on a big triangle on \mathbb{C} . The difficulty is that the outermost region of the big triangle is sparse, while the innermost region is extremely dense. Hence, a slight change of the Beltrami differentials at the outermost region will result in undesirably large changes at the innermost region. Consequently, the southern hemisphere of the resulting spherical parameterization will have large distortions. Hence, we have to limit the change of the Beltrami differential at the outermost region. Motivated by the fact that the outermost region of the big triangle corresponds to the region around the

north pole on \mathbb{S}^2 , we propose using the geodesic distance between a point and $(0, 0, 1)$ as the weighting factor.

More explicitly, let $\tilde{\phi}_1^0 : \mathbb{C} \setminus \Omega \rightarrow \mathbb{C}$ be the landmark aligned parameterization obtained from the last subsection. Denote the Beltrami differential of $\tilde{\phi}_1^0$ by ν^0 . First, we chop down $|\nu^0|$ by

$$(4.19) \quad |\tilde{\nu}(z)| = \min\{|\nu^0(z)|, 1 - \epsilon\}$$

for all $z \in \mathbb{C} \setminus \Omega$, where $\epsilon > 0$ is a small constant (usually chosen as 0.01). We then look for a smooth approximation μ_{smooth} of $\tilde{\nu}$ by

$$(4.20) \quad \mu_{smooth}^0 = \mathbf{argmin}_{\mu} \int \left(|\nabla \mu|^2 + |\mu - \tilde{\nu}|^2 + \frac{1}{D} |\mu|^2 \right),$$

where $D : \mathbb{C} \setminus \Omega \rightarrow \mathbb{R}^+$ and $D(p)$ is defined as the geodesic distance between $(0, 0, 1)$ and the image of $p \in \mathbb{C} \setminus \Omega$ under the inverse stereographic projection. Here, $|\nabla \mu|^2$ measures the smoothness of the Beltrami differential, $|\mu - \tilde{\nu}|^2$ measures the difference between the original and the new Beltrami differential, and D gives a weight for limiting the changes of the Beltrami differential for points close to ∞ (which corresponds to the north pole in \mathbb{S}^2).

After μ_{smooth}^0 is computed, we apply the LBS [3] (as described in section 4.1) to reconstruct the quasi-conformal map g^0 with the corresponding Beltrami differential μ_{smooth}^0 with landmarks fixed. Denote the Beltrami differential of g^0 by μ_{lm} . Let $\mu^0 = \mu_{smooth}^0 + t(\mu_{lm} - \mu_{smooth}^0)$, where $t \in [0, 1]$ is the landmark-matching factor. We then compute a quasi-conformal map f^0 with Beltrami differential μ^0 using LBS. This step balances the smoothness and landmark-matching property of the quasi-conformal map f^0 . We then set ν^1 as the Beltrami differential of the map f^0 and set $\tilde{\phi}_1^1 = f^0$. We keep the iteration going until the resulting map $\tilde{\phi}_1^n$ becomes a diffeomorphism.

In summary, the proposed algorithm can be described as follows: supposing that ν^n and $\tilde{\phi}_1^n$ are obtained at the n th iteration, ν^{n+1} and $\tilde{\phi}_1^{n+1}$ can be obtained as follows:

$$(4.21) \quad \begin{aligned} f^n &= \mathbf{LBS}(\mu^n), \\ \nu^{n+1} &= \mu(f^n), \\ \tilde{\phi}_1^{n+1} &= f^{n+1}. \end{aligned}$$

In the discrete case, we can approximate D by the area of triangular faces, denoted by $A(T)$. The rationale behind this is that under the stereographic projection, the triangular faces closer to the north pole will be mapped to a larger triangle on $\bar{\mathbb{C}}$. Hence, $A(T)$ is proportional to $1/D(T)$. The minimizer μ_{smooth}^0 of the optimization problem (4.20) can be obtained by solving the following equation:

$$(4.22) \quad \Delta \mu_{smooth}^0 + (1 + A(T)) \mu_{smooth}^0 = \nu.$$

After a bijective map $\tilde{\phi}_1 : \mathbb{C} \setminus \Omega \rightarrow \mathbb{C} \setminus \Omega$ is obtained, a bijective landmark aligned spherical parameterization of S_1 can be achieved by $\phi_1^* := P_N^{-1} \circ \tilde{\phi}_1 \circ \phi_1$. Again, one drawback of this algorithm is that there are large conformality distortions around the north pole. Thus, the

Beltrami differential near the north pole is big. In contrast, the Beltrami differential of the region near the south pole will be approximately 0 (negligible). To correct the distortions, we again composite the map with a quasi-conformal map. First, we apply the south pole stereographic projection to map \mathbb{S}^2 to \mathbb{C} . Then we compute the Beltrami differential μ of the map from the plane to the original cortical surface. We fix the landmark positions and also the region in \mathbb{C} that corresponds to a small region enclosing the south pole, and then apply LBS [3] to reconstruct the quasi-conformal map using the same Beltrami differential μ . By Theorem 4.1, the conformality distortions are corrected. Also, the positions of the landmarks are fixed by our setup.

5. Numerical implementation. In this section, the numerical implementation details will be explained. Let K_1, K_2 be the triangulations of two cortical surfaces S_1 and S_2 , respectively. Denote the edge spanned by two vertices u, v by $[u, v]$, and the landmarks on the surfaces by $\{p_i\}_{i=1}^n$ and $\{q_i\}_{i=1}^n$, respectively, with p_i matching q_i .

The discrete harmonic energy is given by

$$(5.1) \quad E(\varphi) = \sum_{[u,v] \in K} k_{uv} \|\varphi(u) - \varphi(v)\|^2.$$

Here $k_{uv} = \cot \alpha + \cot \beta$, where α, β are the angles opposite to the edge $[u, v]$. The discrete Laplacian is given by

$$(5.2) \quad \Delta\varphi = \sum_{[u,v] \in K} k_{uv} (\varphi(u) - \varphi(v)).$$

For landmark aligned harmonic parameterization, the discrete form of the combined energy functional proposed in [2, 30] is

$$(5.3) \quad E_{combined}(\varphi) = \sum_{[u,v] \in K_1} k_{uv} \|\varphi(u) - \varphi(v)\|^2 + \lambda \sum_{i=1}^n \|\varphi(p_i) - q_i\|^2,$$

where λ is a weighting factor. The discrete Laplacian of the energy is given by

$$(5.4) \quad \Delta\varphi = \sum_{[u,v] \in K_1} k_{uv} (\varphi(u) - \varphi(v)) + \lambda \sum_{u \in K_1} (\varphi(u) - q_i) \chi_{K_1}(u).$$

In our algorithms, we apply the LBS proposed in [3] to reconstruct a quasi-conformal map from a given Beltrami differential with fixed vertex locations of the big triangle. We denote the obtained quasi-conformal map with respect to the Beltrami differential μ by $\mathbf{LBS}(\mu)$. In particular, if landmark constraints are enforced, we denote the map by $\mathbf{LBS}_{LM}(\mu)$. For the implementation of LBS, please refer to [3]. We abbreviate the name of our proposed method as FLASH, which refers to fast landmark aligned spherical harmonic parameterization.

5.1. Fast spherical conformal parameterization of genus-0 closed surfaces. The numerical implementation details of our proposed fast algorithm to compute the spherical conformal parameterization are described in Algorithm 1. A graphical illustration of the proposed algorithm is also given in Figure 2.

Algorithm 1: Spherical conformal parameterization of genus-0 closed surfaces.

Input: A genus-0 closed cortical surface mesh K .

Output: A spherical conformal parameterization $\phi : K \rightarrow \mathbb{S}^2$.

- 1 Remove a triangular face $T_k = [v_{k_1}, v_{k_2}, v_{k_3}]$ on the brain mesh K . Choose a big triangle $[b_1, b_2, b_3]$ on \mathbb{C} with the optimal size that shares the same angle structure with $T_k = [v_{j_1}, v_{j_2}, v_{j_3}]$. In practice, we choose the most regular triangular face of the mesh. This is because an irregular boundary big triangle may affect the conformality of the result of step 2;
- 2 A conformal parameterization $\varphi : K \setminus \{T_k\} \rightarrow \mathbb{C}$ can be obtained by solving the sparse linear system

$$\begin{cases} \sum_{[u,v] \in K} k_{uv}(\varphi(u) - \varphi(v)) = 0 & \text{if } u \neq v_{j_1}, v_{j_2}, v_{j_3}, \\ \varphi(v_{j_t}) = b_t & \text{if } t = 1, 2, 3; \end{cases}$$

Obtain the spherical mesh by the inverse stereographic projection;

- 3 Project the sphere onto \mathbb{C} through the south pole stereographic projection P_S . Denote the result as D ;
 - 4 Compute the Beltrami differential μ of the map $f : D \rightarrow K$;
 - 5 Compute $g = \mathbf{LBS}(\mu)$ with a small region around the south pole fixed;
 - 6 Project the plane to \mathbb{S}^2 by the inverse south pole stereographic projection P_S^{-1} ;
 - 7 Obtain the spherical conformal parameterization $\phi := P_S^{-1} \circ g \circ P_S \circ P_N^{-1} \circ \varphi$;
-

Algorithm 2: Landmark aligned harmonic map.

Input: Two genus-0 closed cortical surface meshes S_1, S_2 and the weight λ .

Output: A landmark aligned harmonic map φ on the complex plane.

- 1 Apply Algorithm 1 to two cortical surface meshes S_1 and S_2 and obtain two spherical meshes B_1 and B_2 , respectively;
- 2 Apply a Möbius transformation f to B_1 of the form $f(z) = az + b$ which minimizes the landmark mismatch energy $\sum_{i=1}^n |f(z_i) - w_i|^2$, where $\{z_i \in \mathbb{C}\}, \{w_i \in \mathbb{C}\}$ are the landmarks of B_1, B_2 under the stereographic projection [1]. Denote the resulting spherical mesh by \tilde{B}_1 ;
- 3 Project \tilde{B}_1, B_2 onto \mathbb{C} by the stereographic projection P_N ;
- 4 Obtain the landmark constrained harmonic map φ on \mathbb{C} by solving the sparse linear system

(5.5)

$$\begin{cases} \sum_{[u,v] \in K} k_{uv}(\varphi(u) - \varphi(v)) + \lambda(\varphi(u) - q_i) = 0 & \text{if } u = p_i, i = 1, 2, \dots, n, \\ \sum_{[u,v] \in K} k_{uv}(\varphi(u) - \varphi(v)) = 0 & \text{if } u \notin \{p_1, p_2, \dots, p_n, j_1, j_2, j_3\}, \\ \varphi(v_{j_t}) = v_{j_t} & \text{if } t = 1, 2, 3; \end{cases}$$

Here $\{p_i\}_{i=1}^n, \{q_i\}_{i=1}^n$ are the landmarks of the meshes on \mathbb{C} ;

Algorithm 3: Preservation of bijectivity via Beltrami differentials.

Input: Two meshes S_1, S_2 , the spherical conformal parameterization $\phi_1 : S_1 \rightarrow \tilde{B}_1$, and the optimized harmonic map $\varphi : P_N(\tilde{B}_1) \rightarrow \mathbb{C}$.

Output: A bijective landmark aligned spherical harmonic parameterization.

- 1 Compute the Beltrami differential ν of the map $\psi : \varphi(P_N(\tilde{B}_1)) \rightarrow S_1$;
 - 2 **repeat**
 - 3 Compute

$$\mu_{smooth} := \operatorname{argmin}_{\mu} \int (|\nabla\mu|^2 + |\mu - \nu|^2 + A(T)|\mu|^2),$$
 where $A(T)$ is the area of the triangular face T on the plane. This can be done by solving $\Delta\mu + (1 + A(T))\mu = \nu$;
 - 4 For every triangular face T , chop down the norm of $\mu_{smooth}(T)$ by $|\mu_{smooth}(T)| := \min\{|\mu_{smooth}(T)|, 0.99\}$;
 - 5 Compute $g = \mathbf{LBS}_{LM}(\mu_{smooth})$;
 - 6 Compute the Beltrami differential μ_{lm} of g ;
 - 7 Define $\mu := \mu_{smooth} + t(\mu_{lm} - \mu_{smooth})$, where $t \in [0, 1]$ is the landmark-matching factor;
 - 8 For every triangular face T , chop down the norm of $\mu(T)$ by $|\mu(T)| := \min\{|\mu(T)|, 0.99\}$;
 - 9 Compute $f = \mathbf{LBS}(\mu)$;
 - 10 Update ν by the Beltrami differential of f ;
 - 11 **until** *The resulting map is bijective*;
 - 12 Obtain the spherical mesh using the inverse stereographic projection;
 - 13 Project the sphere onto $\bar{\mathbb{C}}$ through the south pole stereographic projection P_S . Denote the result as D ;
 - 14 Compute the Beltrami differential μ_D of the map $f_D : D \rightarrow K_1$;
 - 15 Compute $g_D = \mathbf{LBS}_{LM}(\mu_D)$ with a small region around the south pole fixed;
 - 16 Project the plane to \mathbb{S}^2 by the inverse south pole stereographic projection P_S^{-1} ;
 - 17 Obtain the desired parameterization $P_S^{-1} \circ g_D \circ P_S \circ P_N^{-1} \circ f \circ \varphi \circ P_N \circ \phi_1$;
-

5.2. Landmark aligned harmonic parameterization. In this subsection, the numerical implementation details of our proposed algorithm for landmark aligned harmonic parameterization, as explained in section 4.2, are described in Algorithm 2.

With the aid of Algorithm 2, a landmark aligned harmonic map on \mathbb{C} can be obtained. However, flips or overlaps may occur in the resulting map.

5.3. Preservation of bijectivity via Beltrami differentials. The implementation details of the proposed iterative algorithm in subsection 4.3 are described in Algorithm 3. The complete procedure of FLASH is illustrated in Figure 3.

6. Experimental results. In this section, we demonstrate the effectiveness of our proposed algorithm for landmark aligned spherical harmonic parameterizations for genus-0 closed cortical surfaces. We perform experiments on 38 pairs of right hemispheric brain surfaces. The

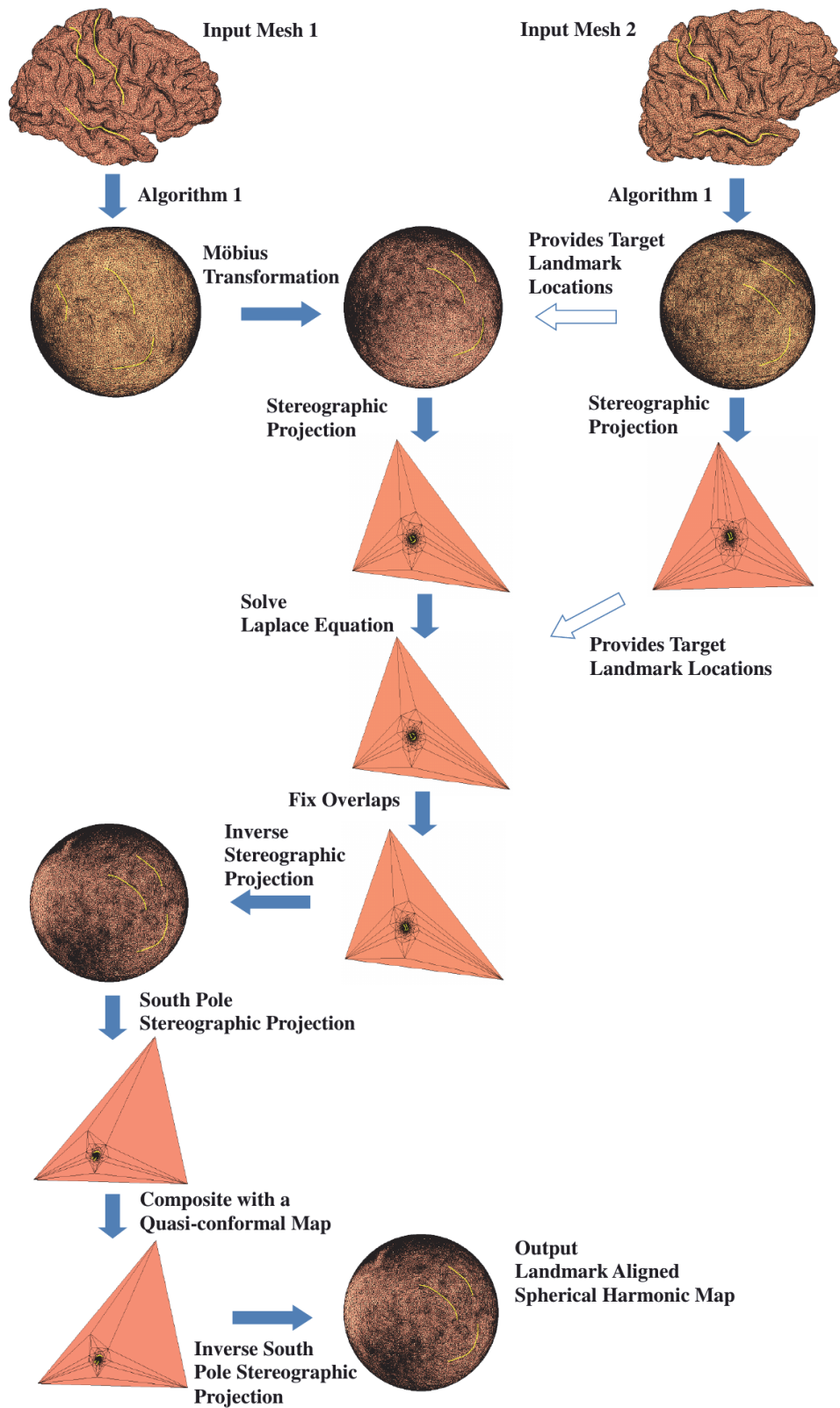


Figure 3. Illustration of the FLASH algorithm.



Figure 4. Spherical conformal parameterizations using our proposed Algorithm 1. Left: Three input brain cortical surfaces. Right: The spherical conformal parameterizations obtained by our proposed Algorithm 1.

cortical surfaces are reconstructed from MRI images of older adult subjects, ages 60–96, using the open source reconstruction software FreeSurfer (<http://surfer.nmr.mgh.harvard.edu/>). Half of the subjects are characterized as nondemented, and half are with dementia of the Alzheimer’s type. The MRI images are freely available from the Open Access Series of Imaging Studies (OASIS) [29]. Each of the reconstructed cortical surfaces consists of about 45,000 vertices and 90,000 faces. On each cortical surface, six landmark curves are manually labeled, including Central Sulcus (CS), Postcentral Sulcus (PostCS), Superior Frontal Sulcus (SFS), Inferior Frontal Sulcus (IFS), Superior Temporal Sulcus (STS), and Inferior Temporal Sulcus (ITS). We first compare our proposed Algorithm 1 for spherical conformal parameterization with the existing algorithms in [1] and [9, 13]. Then for landmark aligned registration, we compare the performance of FLASH with the algorithms in [2], [1], and [16]. All experiments are performed on a PC with a 3.20 GHz CPU.

6.1. Spherical conformal parameterization for cortical surfaces. In our first experiment, we test our proposed fast algorithm for spherical conformal parameterization on the cortical surface data. Figure 4 shows three of the cortical surfaces from our dataset and their parameterizations obtained by our proposed Algorithm 1.

To evaluate our proposed algorithm, we compare the results with two existing algorithms

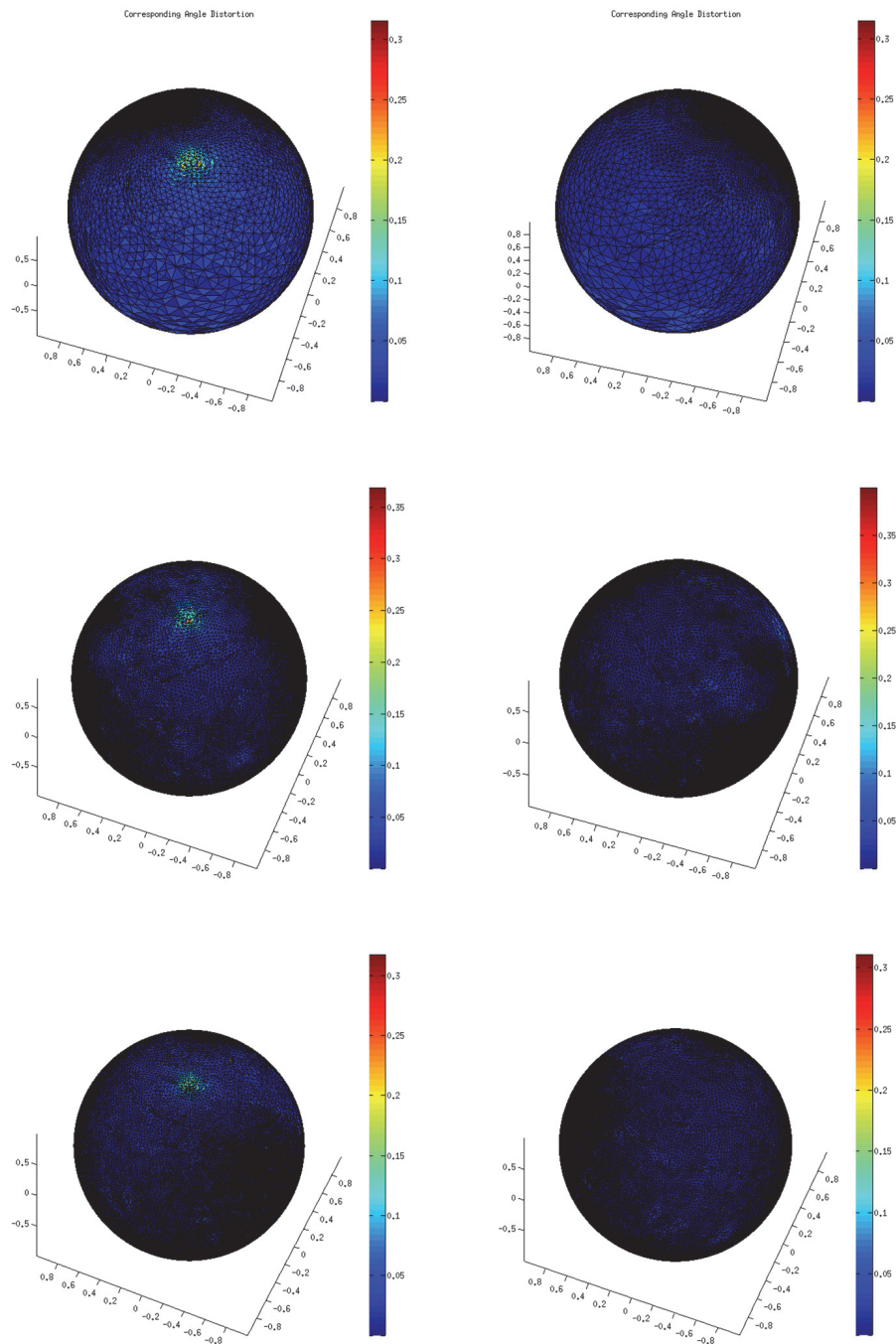


Figure 5. Comparisons between the spherical conformal parameterizations by the algorithm in [9, 13] and our proposed Algorithm 1. Each row represents the results of one brain sample. The colormaps are based on the CDI. It is observed that conformality distortions are induced near the north pole using the algorithm in [9, 13]. The distortions are corrected using our proposed Algorithm 1. Left: The results of the algorithm [9, 13]. Right: The results of our proposed Algorithm 1.

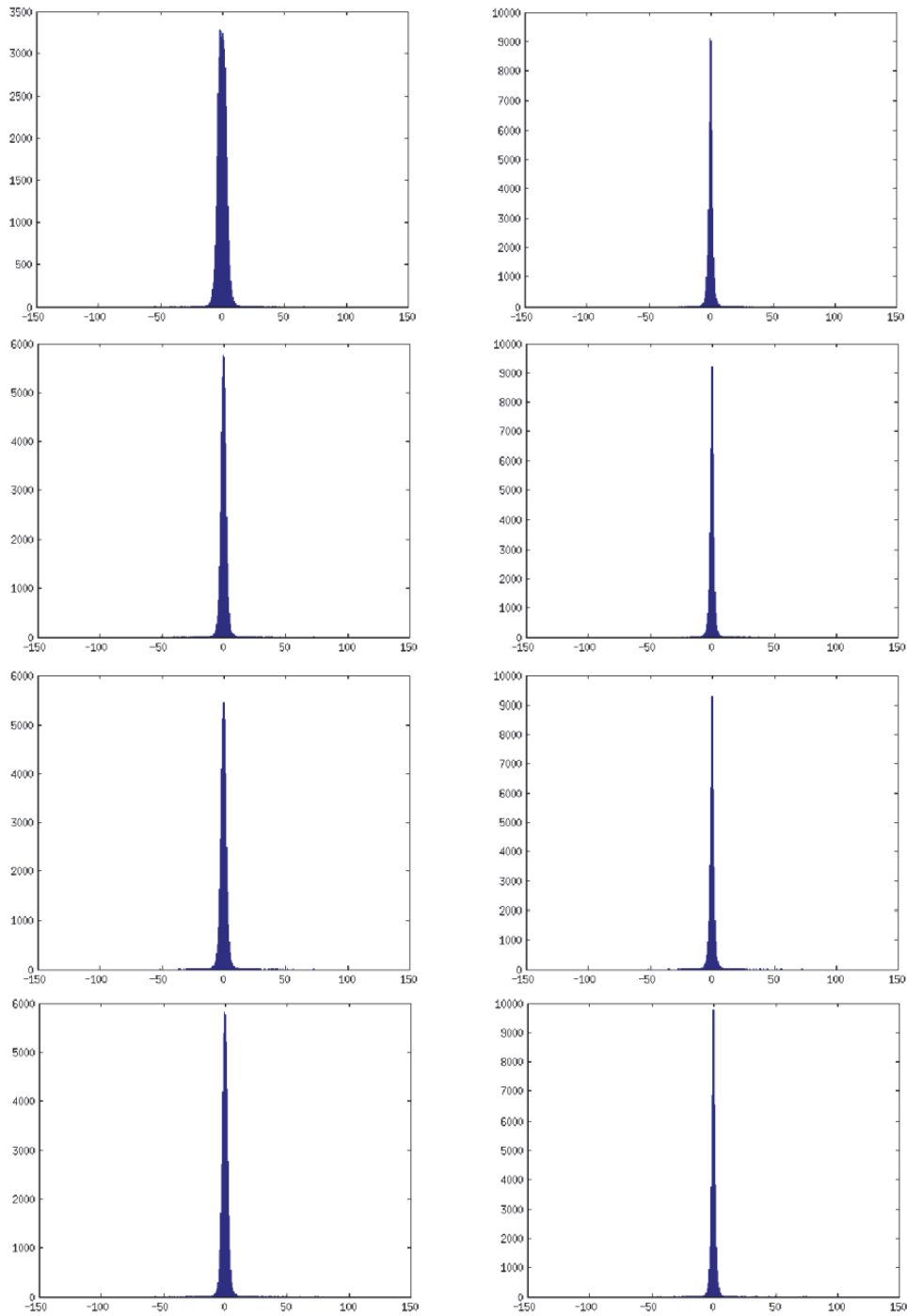


Figure 6. Histograms of angular distortions under the parameterizations obtained by the algorithm in [9, 13] and our proposed Algorithm 1. Each row represents the results of one brain sample. The angular distortions are significantly improved using our proposed Algorithm 1. Left: The histograms of angular distortions under the parameterizations obtained using the algorithm in [9, 13]. Right: The histograms of angular distortions under the parameterizations obtained using our proposed Algorithm 1.

Table 2*Computational time of different algorithms for spherical conformal parameterizations.*

Surface	Time spent (seconds)/mean CDI		
	Algorithm [1]	Algorithm [9, 13]	Our proposed Algorithm 1
Brain 18	6394.50/0.0241	0.4367/0.0128	0.9707/0.0107
Brain 21	6838.46/0.0240	0.4431/0.0216	1.0194/0.0105
Brain 36	5984.28/0.0237	0.4548/0.0142	0.9846/0.0101
Brain 16	7197.37/0.0256	0.4507/0.0149	0.9849/0.0109
Brain 14	7476.53/0.0248	0.4783/0.0148	1.0664/0.0103

in [1] and [9, 13]. We first compare the conformality distortions of the parameterization results obtained by the algorithm proposed in [9, 13] with those by our proposed Algorithm 1. To evaluate the conformality distortion of the algorithms, we define the conformality distortion index (CDI) on each triangular face by $(|\alpha - \alpha'| + |\beta - \beta'| + |\gamma - \gamma'|)/2\pi$, where α, β, γ are the three angles of the resulting triangular face and α', β', γ' are those on the original triangular face. The CDI measures the changes of the angles on each triangular face under the parameterization. As shown in Figure 5, serious conformality distortions near the north pole can be observed for the method in [9, 13]. In contrast, our proposed Algorithm 1 effectively corrects the conformality distortions near the pole. In Figure 6, the contrasts between the angular distortions of the method in [9, 13] and our proposed Algorithm 1 also show that our proposed algorithm possesses lower overall angular distortions.

Table 2 shows the performances of our proposed method and the algorithms proposed in [1] and [9, 13]. The parameters we used to run the algorithm in [1] are time step $\delta t = 0.1$, Tuzé embedding energy threshold = 0.001, and harmonic energy threshold = 0.00001. Our algorithm takes about 1 second on average to obtain the spherical conformal parameterization, which is more than 5000 times faster than the existing algorithm in [1]. Also, with speed comparable to that in [9, 13], our algorithm demonstrates more than 30% improvement in conformality distortions on average. These experimental results reflect the advantages of our proposed method.

6.2. Fast landmark aligned spherical harmonic parameterization for cortical surfaces.

Next, we carry out experiments to test our proposed algorithm FLASH for computing the landmark aligned spherical harmonic parameterizations of cortical surfaces (with $\lambda = 3$). Figure 7 shows the sulci selected as landmark constraints. Figure 8 illustrates the landmark aligned spherical parameterization results obtained by FLASH. It can be observed that the landmarks are well aligned. Figure 9 demonstrates the difference between landmark-free cortical registration and the registration obtained using FLASH, which gives an optimized harmonic registration between the cortical surfaces with landmarks aligned.

Next, as our proposed method for landmark aligned spherical harmonic parameterization is based on the model by Lui et al. [2], we compare the performance of our proposed algorithm FLASH with the algorithm proposed in [2]. We compare the performance in three different aspects.

First, we compare the bijectivity of the parameterizations. Figure 10 compares the registration results obtained from FLASH and the algorithm in [2]. As shown in the figure, flips or foldings can be found for the algorithm in [2]. In contrast, using FLASH, foldings can al-

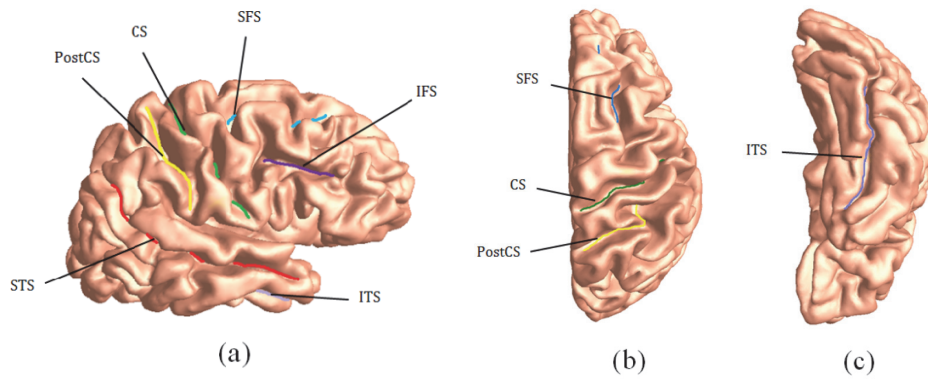


Figure 7. The six sulcal landmarks selected on a right hemispheric brain surface. (a) shows the lateral view of a brain. (b) shows the top view. (c) shows the bottom view.

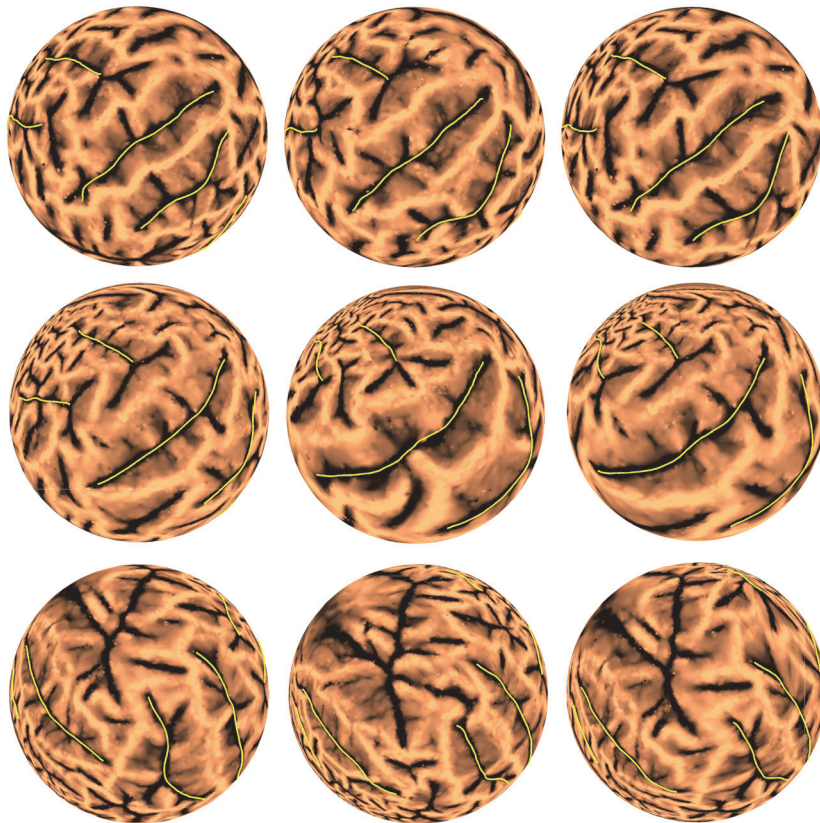


Figure 8. Landmark aligned spherical harmonic parameterizations using FLASH. One set of experimental results is shown in each row. The spherical conformal parameterizations of the source brains and the target brains are shown, respectively, in the first and the second column. The corresponding landmark aligned spherical harmonic parameterizations (with $\lambda = 3$) are given in the third column.

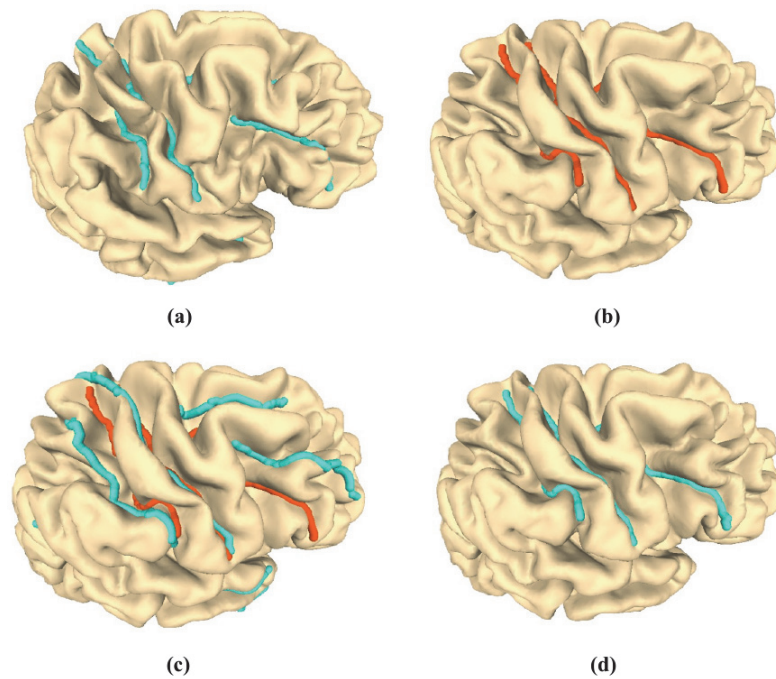


Figure 9. Two cortical surfaces and the registration results. The sulcal landmarks are highlighted. (a) and (b) show the source cortical surface and the target cortical surface, respectively. (c) shows the conformal registration without any landmark constraints. One can observe that the landmark curves are not matched. (d) shows the registration obtained using FLASH.

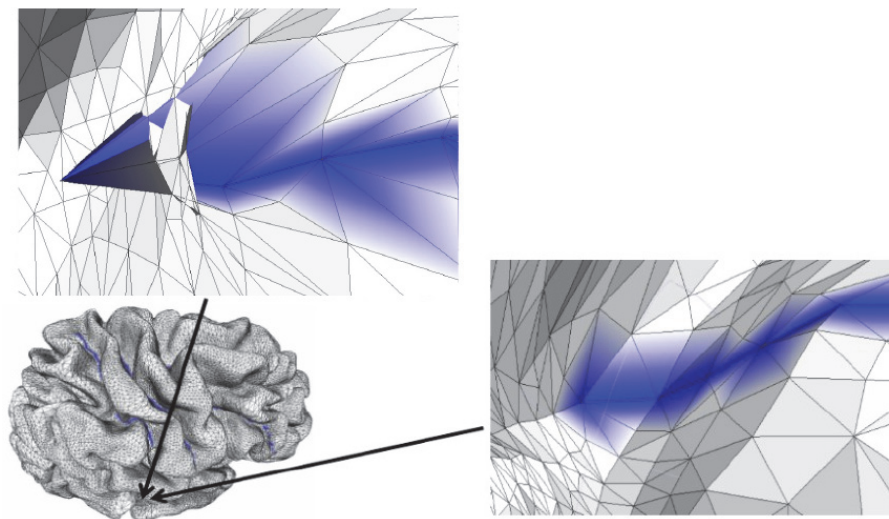


Figure 10. Comparison between the registration results of FLASH and those of the algorithm in [2]. For [2], foldings are observed near a landmark curve (blue). In contrast, FLASH preserves the bijectivity of the registration. Top left: The result of the algorithm in [2]. Bottom right: The result of FLASH.

Table 3

Comparison with the algorithm in [2] for landmark aligned spherical harmonic parameterization.

Surfaces	Algorithm in [2]			FLASH		
	Time spent for landmark matching (seconds)	Number of overlaps	Mean $ \mu $	Time spent (seconds)	Number of overlaps	Mean $ \mu $
Brains 16 and 18	2585	24	0.0755	15.34	0	0.0669
Brains 21 and 35	2921	52	0.0647	16.95	0	0.0696
Brains 13 and 14	2449	133	0.0715	16.44	0	0.0799
Brains 32 and 36	2893	117	0.1047	9.28	0	0.1036
Brains 10 and 8	2837	231	0.0781	16.97	0	0.0822

ways be successfully eliminated. Table 3 lists the number of foldings of the parameterizations obtained by FLASH and the algorithm in [2].

Second, we compare the angular distortions under the parameterizations. Figure 11 illustrates the statistics of the angular distortions of the results obtained by the algorithm in [2] and FLASH. The high similarity of the angular distortion histograms suggests that the global conformality distortion of FLASH is comparable to (sometimes better than) that of the conventional algorithm in [2].

Finally, we compare the computational time. The computational times required by FLASH and the algorithm proposed in [2] are listed in Table 3. Note that for fair comparison, when computing the landmark aligned spherical parameterization using [2], we choose the spherical conformal parameterization as the initialization. In practice, the conventional method in [2] initializes with a Gauss map. Thus, it would probably take longer to converge. Using [2], the time required for landmark matching (excluding the spherical conformal parameterizations of the brain surfaces) is over 40 minutes. In contrast, the time required by FLASH (including the fast spherical conformal parameterizations of the brain surfaces) is usually less than 20 seconds. Hence, the computation of FLASH is over 100 times faster than that of the algorithm in [2].

Besides comparing with the algorithm in [2], we also make comparisons between our proposed FLASH algorithm and two other models for landmark aligned registrations proposed in [1] and [16]. PostCS, ITS, and IFS are used as landmark constraints. Table 4 shows the statistics. Despite the small conformality distortions, the method of [1] suffers from slow computation and large landmark mismatch energy. For the method in [16], although exact landmark matching is enforced, the conformality distortion is relatively large and the bijectivity may be lost. The comparisons demonstrate the advantages of our proposed FLASH algorithm.

7. Conclusions. This paper presents an efficient algorithm, called FLASH, to obtain a bijective landmark aligned spherical harmonic parameterization for genus-0 closed brain surfaces. The three major tasks are (1) speeding up the accurate computation of spherical conformal parameterizations, (2) speeding up the computation of landmark-matching registration, and (3) ensuring the bijectivity of the registration. To solve the first task, we propose

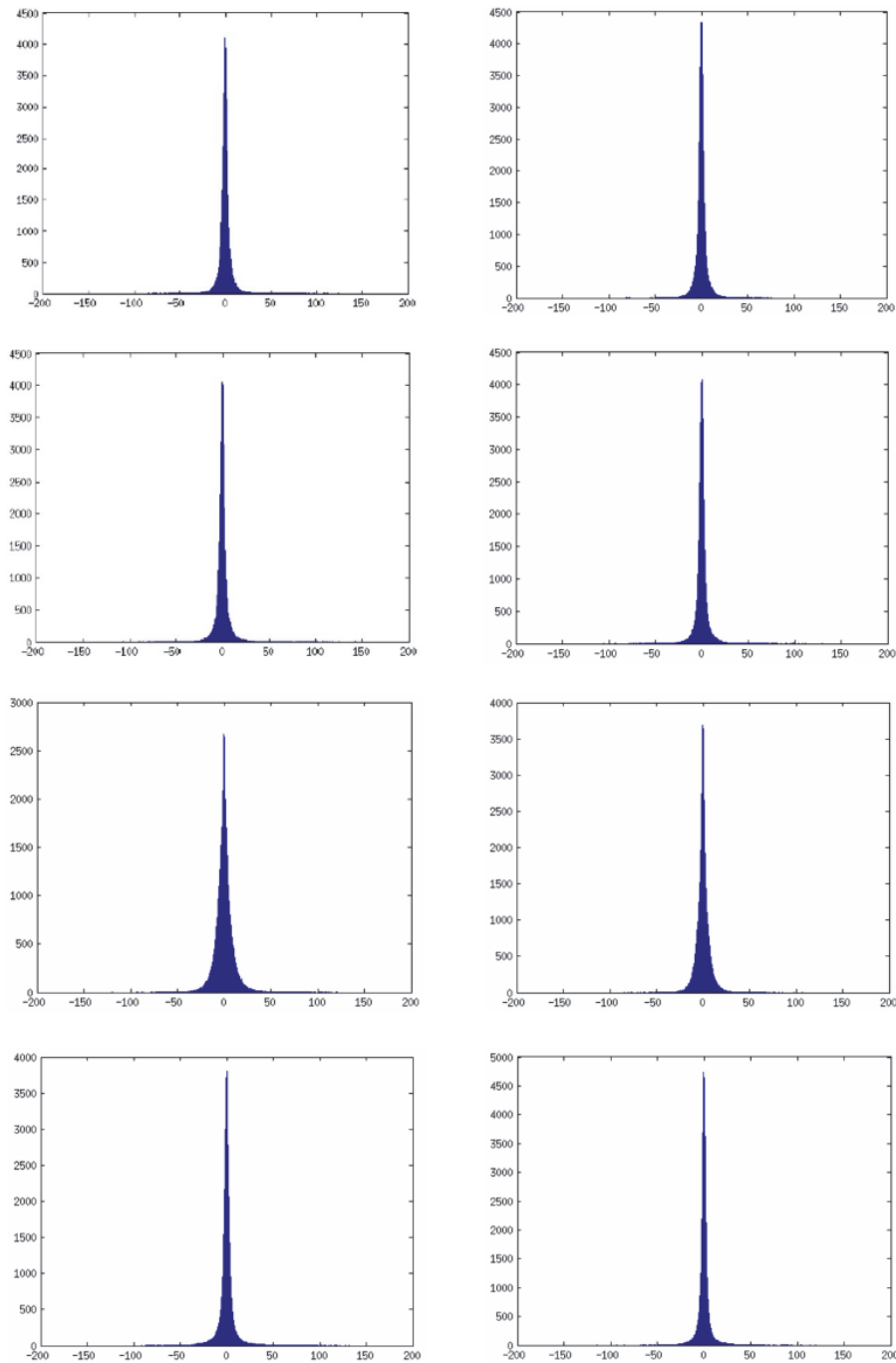


Figure 11. Histograms of angular distortions under the landmark aligned harmonic parameterizations obtained by the algorithm in [2] and those obtained by FLASH. Each row represents the results of one brain pair. Left: The results of the algorithm in [2]. Right: The results of FLASH.

Table 4

Comparison with other algorithms for landmark aligned cortical registrations.

Algorithms	Time spent (seconds)	Number of overlaps	CDI	Landmark mismatch energy
Möbius transformation [1]	13591.88	0	0.0256	2718.19
Shape-based landmark matching [16]	368.25	7	0.0663	0
FLASH ($\lambda = 3$)	5.1455	0	0.0205	113.70

the north pole–south pole iterative scheme to linearize the problem on a big triangle with optimal size and correct the conformality distortion near the north pole. To complete the second task, we formulate the optimization problem proposed in [2] on $\bar{\mathbb{C}}$ and thereby linearize the problem. Finally, by adjusting the Beltrami differential of the mapping, a bijective landmark aligned spherical harmonic parameterization can be easily obtained. With our proposed FLASH algorithm, a diffeomorphic registration between two brain surfaces is efficiently achieved. Experimental results demonstrate the effectiveness of the proposed algorithm. As a remark, our proposed FLASH algorithm can also be effectively applied in the field of computer graphics. For instance, by computing the spherical parameterization using FLASH, the constrained texture mapping of a genus-0 closed surface can be effectively obtained by texturing the spherical parameter space. In the future, we are going to apply the proposed algorithm to more real-life applications.

REFERENCES

- [1] X. GU, Y. WANG, T.F. CHAN, P.M. THOMPSON, AND S.T. YAU, *Genus zero surface conformal mapping and its application to brain surface mapping*, IEEE Trans. Med. Imaging, 23 (2004), pp. 949–958.
- [2] L.M. LUI, Y. WANG, T.F. CHAN, AND P.M. THOMPSON, *Landmark constrained genus zero surface conformal mapping and its application to brain mapping research*, Appl. Numer. Math., 57 (2007), pp. 847–858.
- [3] L.M. LUI, K.C. LAM, T.W. WONG, AND X. GU, *Texture map and video compression using Beltrami representation*, SIAM J. Imaging Sci., 6 (2013), pp. 1880–1902.
- [4] J. EELLS AND L. LEMAIRE, *A report on harmonic maps*, Bull. London Math. Soc., 10 (1978), pp. 1–68.
- [5] J. EELLS AND L. LEMAIRE, *Another report on harmonic maps*, Bull. London Math. Soc., 20 (1988), pp. 385–524.
- [6] U. PINKALL AND K. POLTHIER, *Computing discrete minimal surfaces and their conjugates*, Experiment. Math., 2 (1993), pp. 15–36.
- [7] M. ECK, T. DEROSE, T. DUCHAMP, H. HOPPE, M. LOUNSBERY, AND W. STUETZLE, *Multiresolution analysis of arbitrary meshes*, in Proceedings of the 22nd Annual Conference on Computer Graphics and Interactive Techniques (SIGGRAPH '95), ACM, New York, 1995, pp. 173–182.
- [8] D. ZHANG AND M. HEBERT, *Harmonic maps and their applications in surface matching*, in Proceedings of the IEEE Computer Society Conference on Computer Vision and Pattern Recognition, 1999, pp. 524–530.
- [9] S. ANGENENT, S. HAKER, A. TANNENBAUM, AND R. KIKINIS, *Conformal geometry and brain flattening*, in Medical Image Computing and Computer-Assisted Intervention—MICCAI 1999, Springer-Verlag, Berlin, Heidelberg, 1999, pp. 271–278.
- [10] B. LÉVY, S. PETITJEAN, N. RAY, AND J. MAILLOT, *Least squares conformal maps for automatic texture atlas generation*, ACM Trans. Graph., 21 (2002), pp. 362–371.

- [11] P. ALLIEZ, M. MEYER, AND M. DESBRUN, *Interactive geometry remeshing*, ACM Trans. Graph., 21 (2002), pp. 347–354.
- [12] M.K. HURDAL AND K. STEPHENSON, *Cortical cartography using the discrete conformal approach of circle packings*, NeuroImage, 23 (2004), pp. S119–S128.
- [13] S. HAKER, S. ANGENENT, A. TANNENBAUM, R. KIKINIS, G. SAPIRO, AND M. HALLE, *Conformal surface parameterization for texture mapping*, IEEE Trans. Vis. Comput. Graphics, 6 (2000), pp. 181–189.
- [14] X. GU AND S.-T. YAU, *Computing conformal structures of surfaces*, Commun. Inf. Syst., 2 (2002), pp. 121–146.
- [15] Y. WANG, L.M. LUI, X. GU, K.M. HAYASHI, T.F. CHAN, A.W. TOGA, P.M. THOMPSON, AND S.-T. YAU, *Brain surface conformal parameterization using Riemann surface structure*, IEEE Trans. Med. Imaging, 26 (2007), pp. 853–865.
- [16] L.M. LUI, S. THIRUVENKADAM, Y. WANG, P.M. THOMPSON, AND T.F. CHAN, *Optimized conformal surface registration with shape-based landmark matching*, SIAM J. Imaging Sci., 3 (2010), pp. 52–78.
- [17] R. LAI, Z. WEN, W. YIN, X. GU, AND L.M. LUI, *Folding-free global conformal mapping for genus-0 surfaces by harmonic energy minimization*, J. Sci. Comput., 58 (2014), pp. 705–725.
- [18] R. SHI, W. ZENG, Z. SU, H. DAMASIO, Z. LU, Y. WANG, S.-T. YAU, AND X. GU, *Hyperbolic harmonic mapping for constrained brain surface registration*, in Proceedings of the 2013 IEEE Conference on Computer Vision and Pattern Recognition, 2013, pp. 2531–2538.
- [19] R. SCHOEN AND S.-T. YAU, *Lectures on Differential Geometry*, International Press, Cambridge, MA, 1994.
- [20] R. SCHOEN AND S. T. YAU, *Lectures on Harmonic Maps*, International Press, Cambridge, MA, 1997.
- [21] F. GARDINER AND N. LAKIC, *Quasiconformal Teichmüller Theory*, AMS, Providence, RI, 2000.
- [22] A. FORNITO, S. WHITTLE, S.J. WOOD, D. VELAKOULIS, C. PANTELIS, AND M. YÜCEL, *The influence of sulcal variability on morphometry of the human anterior cingulate and paracingulate cortex*, NeuroImage, 33 (2006), pp. 843–854.
- [23] A. FORNITO, S.J. WOOD, S. WHITTLE, J. FULLER, C. ADAMSON, M.M. SALING, D. VELAKOULIS, C. PANTELIS, AND M. YÜCEL, *Variability of the paracingulate sulcus and morphometry of the medial frontal cortex: Associations with cortical thickness, surface area, volume, and sulcal depth*, Hum. Brain Mapp., 29 (2008), pp. 222–236.
- [24] B. FISCHL, N. RAJENDRAN, E. BUSA, J. AUGUSTINACK, O. HINDS, B.T. YEO, H. MOHLBERG, K. AMUNTS, AND K. ZILLES, *Cortical folding patterns and predicting cytoarchitecture*, Cereb. Cortex, 18 (2008), pp. 1973–1980.
- [25] M.S. MEGA, P.M. THOMPSON, J.L. CUMMINGS, C.L. BACK, M.L. XU, S. ZOHOORI, A. GOLDKORN, J. MOUSSAI, L. FAIRBANKS, G.W. SMALL, AND A.W. TOGA, *Sulcal variability in the Alzheimer’s brain: Correlations with cognition*, Neurology, 50 (1998), pp. 145–151.
- [26] J.S. KIPPENHAN, R.K. OLSEN, C.B. MERVIS, C.A. MORRIS, P. KOHN, A. MEYER-LINDENBERG, AND K.F. BERMAN, *Genetic contributions to human gyrification: Sulcal morphometry in Williams syndrome*, J. Neurosci., 25 (2005), pp. 7840–7846.
- [27] D.C. VAN ESSEN, D. DIERKER, A.Z. SNYDER, M.E. RAICHLER, A.L. REISS, AND J. KORENBERG, *Symmetry of cortical folding abnormalities in Williams syndrome revealed by surface-based analyses*, J. Neurosci., 26 (2006), pp. 5470–5483.
- [28] B. FISCHL, M.I. SERENO, AND A.M. DALE, *Cortical surface-based analysis. II: Inflation, flattening, and a surface-based coordinate system*, NeuroImage, 9 (1999), pp. 195–207.
- [29] D.S. MARCUS, A.F. FOTENOS, J.G. CSERNANSKY, J.C. MORRIS, AND R.L. BUCKNER, *Open access series of imaging studies: Longitudinal MRI data in nondemented and demented older adults*, J. Cogn. Neurosci., 22 (2010), pp. 2677–2684.
- [30] Y. WANG, L.M. LUI, T.F. CHAN, AND P.M. THOMPSON, *Optimization of brain conformal mapping with landmarks*, in Medical Image Computing and Computer-Assisted Intervention—MICCAI 2005, Part II, Springer-Verlag, Berlin, Heidelberg, 2005, pp. 675–683.
- [31] L.M. LUI AND C. WEN, *Geometric registration of high-genus surfaces*, SIAM J. Imaging Sci., 7 (2014), pp. 337–365.
- [32] P.M. THOMPSON AND A.W. TOGA, *A surface-based technique for warping three-dimensional images of the brain*, IEEE Trans. Med. Imaging, 15 (1996), pp. 402–417.
- [33] A.A. JOSHI, D.W. SHATTUCK, P.M. THOMPSON, AND R.M. LEAHY, *Surface constrained volumetric brain registration using harmonic mappings*, IEEE Trans. Med. Imaging, 26 (2007), pp. 1657–1669.

-
- [34] G. AUZIAS, O. COLLIOT, J. GLAUNÈS, M. PERROT, J. MANGIN, A. TROUVE, AND S. BAILLET, *Diffeomorphic brain registration under exhaustive sulcal constraints*, IEEE Trans. Med. Imaging, 30 (2011), pp. 1214–1227.
 - [35] S. DURRLEMAN, X. PENNEC, A. TROUVÉ, AND N. AYACHE, *Measuring brain variability via sulcal lines registration: A diffeomorphic approach*, in Medical Image Computing and Computer-Assisted Intervention—MICCAI 2007, Part I, Springer-Verlag, Berlin, Heidelberg, 2007, pp. 675–682.
 - [36] S.H. JOSHI, R.P. CABEEN, A.A. JOSHI, B. SUN, I. DINOVI, K.L. NARR, A.W. TOGA, AND R.P. WOODS, *Diffeomorphic sulcal shape analysis on the cortex*, IEEE Trans. Med. Imaging, 31 (2012), pp. 1195–1212.